JOURNAL OF SOLID STATE CHEMISTRY 6, 126–135 (1973)

Investigation of the Defect Manganese Silicide Mn_nSi_{2n-m}

LIONEL M. LEVINSON

General Electric Corporate Research and Development, Schenectady, New York 12301

Received April 6, 1972

Low-temperature magnetization studies upon melt-grown single crystals of the defect manganese silicide Mn_nSi_{2n-m} have shown this material to contain small quantities of plate-like MnSi precipitates. Metallographic and electron microprobe analyses have confirmed this result. The strongly magnetic MnSi precipitates dominate the diamagnetic Mn_nSi_{2n-m} matrix, and are responsible for the magnetic behavior reported in the literature. MnSi is metallic, and the plate-like metallic precipitates degrade the thermoelectric efficiency of the degenerate semiconductor Mn_nSi_{2n-m}.

1. Introduction

The properties of transition metal silicides have attracted interest due to their general relevance to silicon technology (*1*, *2*). A number of disilicides are moreover degenerate semiconductors, and have been extensively investigated as promising refractory, special-purpose thermoelectric elements (*3–6*). The most silicon-rich silicide of manganese, Mn_nSi_{2n-m}, having the approximate composition $MnSi_{1.72}$, has been shown (*7–9*) to be a *p*-type degenerate semiconductor. Its band gap (*9*) is believed to be around 0.8 eV, although details of the band structure are unknown.

Our interest in this material was aroused by the reported magnetic behavior of the compound. Radovskiy et al. (*10*) and Korshunov (*11*) reported a weak, Curie–Weiss type, room-temperature paramagnetism, with a stoichiometry-dependent, large θ (~100°K). This was interpreted as indicative of the presence of both Mn^{5+} and Mn^{4+} in Mn_nSi_{2n-m}, the former ion being in a zero-spin state and the latter having spin $\frac{1}{2}$. Shinoda and Asanabe (*12*) have claimed single crystals of the compound to be metamagnetic.

In light of the above, we have undertaken low-temperature magnetic measurements on melt-grown single crystals of Mn_nSi_{2n-m}, with a view to elucidating the magnetic properties of this compound.

Briefly, we may summarize our results by the statement that melt-grown Mn_nSi_{2n-m} is in fact diamagnetic. The magnetic properties previously ascribed (*10–12*) to Mn_nSi_{2n-m} are incorrect, since as-cast and single-crystal material contain varying amounts (~2 wt %) of the strongly magnetic compound MnSi. The presence of plate-like MnSi precipitates seems to be intrinsic to melt-grown Mn_nSi_{2n-m}, and their appearance is probably independent of melt composition, growth rate, or annealing. Since MnSi is metallic, and Mn_nSi_{2n-m} a semiconductor, we may also expect the precipitate to have substantial effects upon the electrical properties of Mn_nSi_{2n-m}, and we attempt to estimate these effects.

Before proceeding to an outline of the work undertaken, we will, as a convenience for the reader, summarize some details regarding the crystal structure of Mn_nSi_{2n-m} and the Mn–Si phase diagram.

A series of X-ray diffraction (*13–15*) and electron diffraction (*16*) studies of manganese silicide single crystals has indicated the existence of several closely related phases in the composition range $MnSi_{1.71}$–$MnSi_{1.75}$. The tetragonal unit cell of the structure contains *n* tetragonal pseudocells of a β-Sn-like arrangement of Mn atoms stacked along the *c*-direction. The structure can be derived from the $TiSi_2$-type structure, upon replacing the Ti atoms by Mn to form the tetragonal subcell, while appropriately stretching the silicon atoms along the *c*-axis so as to decrease the number of Si atoms per Mn atom. The compound is designated by the formula Mn_nSi_{2n-m}, *n* representing the number of subcells

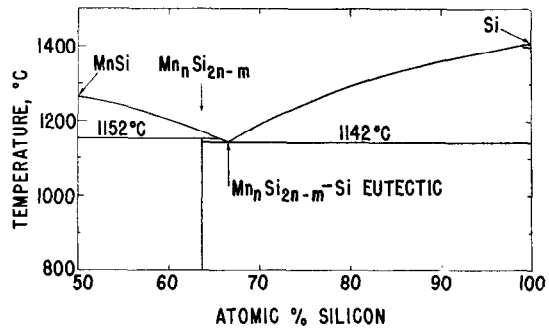

FIG. 1. Phase diagram of MnSi–Si, according to Mager and Wachtel (*19*).

along the *c*-axis for the particular superlattice in question. The conditions controlling the formation of a particular superstructure are not known (*16*). Prolonged annealing has no effect. Single crystal-structure determinations have been performed on crystal fragments corresponding to Mn_4Si_7 (*13*), $Mn_{27}Si_{47}$ (*15*), and $Mn_{15}Si_{26}$ (*14*). Illustrations of the $Mn_{15}Si_{26}$ superstructure may be found in Ref. (*14*).

A series of recent studies (*17–19*) have been undertaken to elucidate the nature of the Mn–Si phase diagram in the vicinity of the compound Mn_nSi_{2n-m}. While Fujino et al. (*17*) claim Mn_nSi_{2n-m} to melt congruently, Morokhovets et al. (*18*) and Mager and Wachtel (*19*) find a peritectic reaction between liquid and MnSi to form Mn_nSi_{2n-m}. Our metallographic data support the latter view (see Section 4), and in Fig. 1 we reproduce the phase diagram according to Mager and Wachtel (*19*).

This article is arranged as follows: In Section (2) we describe crystal growth of Mn_nSi_{2n-m}, and in Section (3) the magnetic characterization of this material is discussed. Section (4) details the results of metallographic and electron microprobe studies. Section (5) is devoted to our magnetic measurements upon the Mn_nSi_{2n-m}—Si eutectic (see Fig. 1). In Section (6) we discuss the implications of the presence of plate-like MnSi precipitates upon the electrical and thermal properties of Mn_nSi_{2n-m}, and Section (7) contains a discussion of the probable mechanism for the origin of the observed MnSi precipitates.

2. Crystal Growth

Starting materials for the growth of Mn_nSi_{2n-m} single crystals were 99.99% manganese flake[1] and 100 Ω-cm, *n*-type, semiconductor grade silicon[2]. Melt compositions ranged from $MnSi_{1.69}$ to $MnSi_{2.00}$. The elemental Mn and Si were prereacted by induction heating in a water-cooled copper boat (*20*) under dry, gettered argon. The resulting ingot was placed in a thin-walled (≈0.020 in.) pointed quartz crucible, which was in turn placed in a close-fitting, supporting Mullite sheath. Crystal growth followed the usual Bridgman technique, the crucible being slowly lowered out of the hot zone of a resistively heated platinum–rhodium furnace. An atmosphere of dry, gettered argon was provided for crystal growth. Weight loss after premelting or after crystal growth was less than 0.01%. Growth rates of 2 mm/hr were typical, and crack-free boules of about 1 cm diameter by 4 cm long were obtained.

The boules were sectioned and polished for metallographic examination. X-ray powder diffraction analysis of the middle of the boule verified the presence of Mn_nSi_{2n-m}. No lines corresponding to another phase could be discerned. Laue back-reflection photographs indicated the material to be single crystal.

We have made no attempt to verify which particular superstructure or superstructures our growth method produced. (Crystals produced by a Czochralski technique (*21*) have been identified as $Mn_{27}Si_{47}$.) It is possible that the magnetic or thermoelectric properties of Mn_nSi_{2n-m} vary somewhat with the superlattice. However, both our measurements and those reported by numerous workers in the literature (*7–12, 17*) agree qualitatively, and presumably correspond to various superlattice structures. The object of this paper is to show that the reported properties are influenced or dominated by the presence of MnSi precipitates. While the growth parameter dependence of the Mn_nSi_{2n-m} superlattice type and the detailed behavior of various physical properties upon superlattice structure are of intrinsic interest, these questions are not addressed here.

3. Magnetic Measurements

The semiconducting transition metal disilicides $FeSi_2$ and $CrSi_2$ (*22, 23*) are weakly diamagnetic at room temperature and exhibit a Pauli paramagnetic contribution at higher temperatures upon exciting sufficient electrons into the conduction band. This is to be contrasted with the

[1] Supplied by Gallard–Schlesinger Chemical Corporation.

[2] Supplied by Dow Corning Corporation.

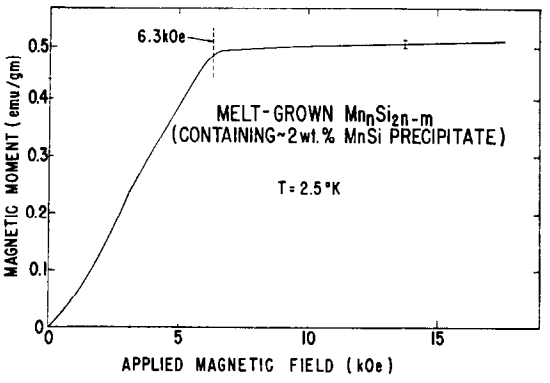

FIG. 2. Magnetization of melt-grown Mn_nSi_{2n-m} as a function of applied magnetic field at $T = 2.5°K$. The observed behavior results from the presence of about 2 wt % MnSi precipitate. Mn_nSi_{2n-m} itself is diamagnetic (Section 5).

semiconducting silicide Mn_nSi_{2n-m} which has been reported (*10, 11*) as exhibiting a Curie–Weiss type paramagnetism and low-temperature metamagnetism (*12*).

We have undertaken magnetization measurements upon Mn_nSi_{2n-m} using a Foner-type vibrating sample magnetometer. Melt-grown single crystals sectioned from the middle of a boule (Section 2) were powdered and measured over the range $2.5°K < T < 300°K$ and $H < 20$ kOe. At room temperature apparent paramagnetic behavior was observed, with susceptibility $\chi = 0.5 \times 10^{-6}$ emu/g, agreeing reasonably well with values in the literature (*10, 12*).

In Fig. 2 we give the measured magnetization as a function of applied magnetic field H at 2.5°K. A number of features are noteworthy. The magnetization is quite linear with H for $H \gtrsim 3$ kOe, with slight departure from linearity for lower fields. At $H = 6.3$ kOe the moment saturates, thereafter increasing very slowly with increasing field. The saturation moment is very low, corresponding to roughly 0.01 μ_B/Mn if we were to distribute the magnetic moment evenly over all the Mn atoms. A Curie temperature determination indicates that $T_c \approx 30°K$.

All the above results are consistent with the hypothesis that melt-grown "single crystal" Mn_nSi_{2n-m} contains about 2 wt % MnSi as an impurity. MnSi is known (*12, 24*) to have $T_c = 30°K$, and to possess a roughly linear magnetization curve up to $H = 6.3$ kOe, where abrupt saturation occurs. We have grown crystals of MnSi and verified that aside from a change of scale in the magnetization, the low temperature magnetic behavior of Mn_nSi_{2n-m} apes that of MnSi. The deviation from linearity observed (Fig. 2) for $H < 3$ kOe is probably indicative of an effect associated with magnetic anisotropy, and will be the subject of a later publication (*25*). Since the room-temperature susceptibility of MnSi is 30×10^{-6} emu/g (*12, 25*), we would also have agreement upon ascribing the measured paramagnetic room-temperature susceptibility of Mn_nSi_{2n-m} ($= 0.5 \times 10^{-6}$ emu/g) to the presence of MnSi precipitates.[3] The above hypothesis is moreover not at variance with the X-ray data as a 2 wt % precipitate would generally remain undetected by X-ray analysis.

We may note at this point that it seems reasonable to expect that the exact amount of MnSi precipitate will vary with the crystal growth conditions and even with position along the boule. We verified this result magnetically for a few specimens, but no extensive investigation has been undertaken. For no combination of melt stoichiometry or crystal growth rate were we able to eliminate the MnSi precipitates, however, and it appears that their presence is inherent in melt-grown Mn_nSi_{2n-m}. Clearly, such variations in the weight fraction of MnSi precipitated would explain the stoichiometry dependence in the susceptibility observed by Radovskiy et al. (*10*).

In an attempt to ascertain the effect of annealing upon the magnetization, a sample was treated in vacuo at 1130°C for 50 hr and then quenched. No change in the low temperature magnetic moment was observed.

We may conclude from the above that Mn_nSi_{2n-m} is either weakly paramagnetic or diamagnetic. In Section 5 we will describe a method to measure the susceptibility of Mn_nSi_{2n-m} as present in the Mn_nSi_{2n-m}–Si eutectic. Before proceeding to those results, however, it is appropriate that we describe metallographic and electron microprobe studies verifying the results of our magnetic measurements.

4. Metallographic and Electron Microprobe Analysis

Boules of Mn_nSi_{2n-m} grown as described in Section 2 were cut and polished using standard

[3] This agreement is much poorer when we include the diamagnetism of Mn_nSi_{2n-m} (Section 5). However, it is probable that the exact value of the diamagnetic susceptibility of Mn_nSi_{2n-m} is stoichiometry-dependent as is the case for $CrSi_2$ (*23*), and the discrepancy is therefore to be expected.

metallographic methods. The final polish was obtained using 0.05 μm alumina. As would be expected from the peritectic formation of Mn_nSi_{2n-m} (Fig. 1), the first portion of the boule to solidify usually contained dendrites of MnSi. The central portion of the boule appeared to be single crystal, and the last portion to solidify invariably contained Mn_nSi_{2n-m}–Si eutectic. Use of very Si-rich melts (e.g., $MnSi_{2.00}$) precluded the formation of MnSi dendrites at the tip of the boule, but the general morphology was otherwise independent of melt composition. The microstructures observed were similar to those found by Morokhovets et al. (*18*).

The central portions of the as-polished boules appeared to be single phase under bright field illumination. However, upon etching the surface in hydrofluoric acid or examination of the as-polished surface in polarized light the presence of fine striations in the crystal could be detected (Figs. 3 and 4). Similar striations were observed by Morokhovets et al. (*18*) and by Ivanova et al. (*7*). The striations correspond to second-phase precipitates, and have the form of platelets or lamellae lying in the (001) plane. The exact epitaxial relation of the MnSi in the Mn_nSi_{2n-m} matrix could probably be determined by electron diffraction techniques, but we have not attempted to evaluate this.

Electron microprobe analysis was then undertaken to determine the nature of the striations. Using this method, the composition of the striations were determined to be 49 ± 1 at. % Mn, 51 ± 1 at. % Si. The same technique showed the Mn_nSi_{2n-m} matrix to have the composition 37 ± 1 at. % Mn, 63 ± 1 at. % Si. These results

FIG. 3. As-grown Mn_nSi_{2n-m} "single crystal" containing plate-like precipitates of MnSi (dark lines) lying in the (001) plane of Mn_nSi_{2n-m}. The precipitate spacing is about 100 μm. As polished sample, polarized light, ×100.

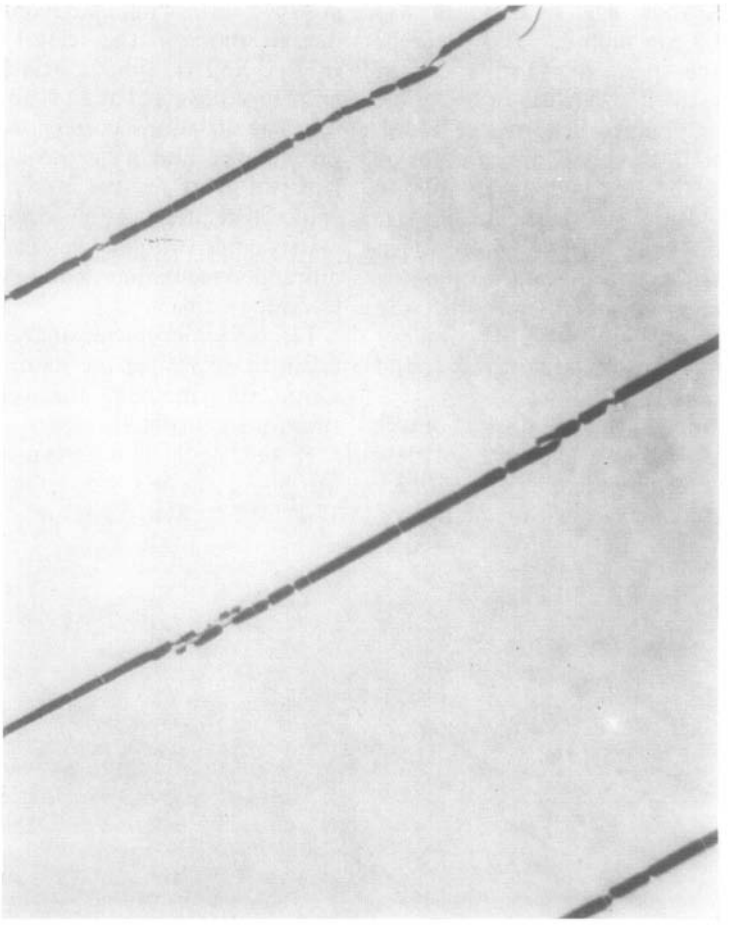

FIG. 4. As Fig. 3, but ×500.

confirm the conclusions drawn from the magnetic measurements described in Section 3.

A further indication of the nature of the striations was forthcoming by comparison of the optical behavior of the striations and that of the MnSi dendrites found at the very tip of some of the boules, as described above. The close color similarity observed under polarized light of these two features is rather convincing.

It is worth emphasizing that the MnSi striations were invariably observed in the "single crystal" portion of the boule, independent of melt composition or growth parameters. Moreover, since MnSi is a metal, the presence of thin, plate-like precipitates can be expected to affect the electrical properties of semiconducting Mn_nSi_{2n-m} and this will be discussed in Section 6. Before proceeding to this topic, however, we shall describe an attempt to evaluate the magnetic properties of Mn_nSi_{2n-m} proper.

5. Magnetic Behavior of Mn_nSi_{2n-m}–Si Eutectic

Metallographic examination of the Mn_nSi_{2n-m}–Si eutectic (Fig. 5) indicated that in this two-phase region, MnSi striations were absent. (The striations persisted right up to the eutectic portion in all the boules examined.) Since Si is weakly diamagnetic, we may expect that the gross features of the magnetic behavior of Mn_nSi_{2n-m} can be ascertained by measurements upon the two-phase material.

Measurements using a Foner-type vibrating sample magnetometer indicated that Mn_nSi_{2n-m} is *diamagnetic*, with $\chi \approx -4 \times 10^{-7}$ emu/g at room temperature. No change was observed on cooling to liquid helium temperature. The correction for the presence of the Si second phase amounted to less than 5%. However, our instrument is not very suited to the measurement of such weak diamagnetic moments, and the number quoted above for χ should be trusted

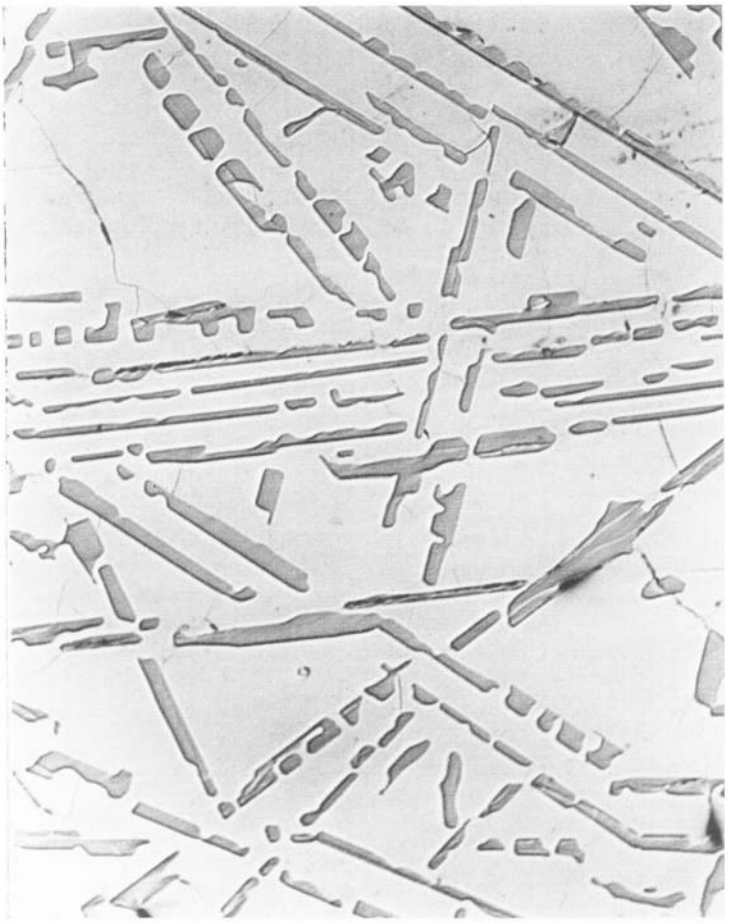

FIG. 5. Mn_nSi_{2n-m}–Si eutectic. As polished, bright field ×100. The matrix is Mn_nSi_{2n-m}, and the darker particles are Si. No MnSi striations were observed, either using polarized light or upon etching in HF (cf. Figs. 3 and 4).

only to within about 20%. It should also be noted that Mn_nSi_{2n-m} has a stoichiometry range (see also Section 7), and we may expect the diamagnetism to vary somewhat with stoichiometry, as is the case for $CrSi_2$ (*23*).

6. Thermoelectric Properties

In Table I we list some room temperature thermal and electrical properties of MnSi and Mn_nSi_{2n-m}. It is evident the MnSi is metallic, with much lower resistivity and thermoelectric power, and higher thermal conductivity, than the degenerate semiconductor Mn_nSi_{2n-m}. Moreover, the thermoelectric properties of Mn_nSi_{2n-m} appear to be very anisotropic. Clearly, however, the presence of oriented plate-like metallic precipitates in Mn_nSi_{2n-m} is of itself sufficient to induce anisotropy.

We may idealize the situation for the electric resistivity as depicted schematically in Fig. 6(a), using a discrete element outline for the current *i*

TABLE I

RESISTIVITY ρ, THERMOELECTRIC POWER α, AND THERMAL CONDUCTIVITY K AT ROOM TEMPERATURE FOR MnSi AND Mn_nSi_{2n-m} CONTAINING MnSi PRECIPITATES

	ρ (milliohm-cm)	α (μV/°K)	K (W/cm-°K)	Reference
MnSi	0.23	34	0.10	(*26*)
	0.15	35	0.13	This work
Mn_nSi_{2n-m}	4.5	160	0.029	(*27*)
$\|c$-axis	6.2	170	0.021	(*7*)
	4.6	170	0.030	This work
Mn_nSi_{2n-m}	1.3	100	0.046	(*27*)
$\perp c$-axis	1.3	105	0.043	(*7*)
	0.94	100	0.054	This work

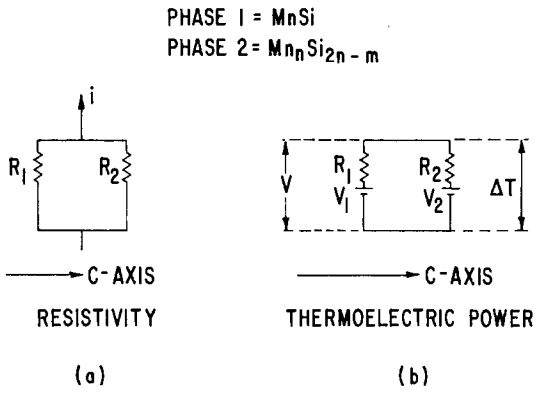

FIG. 6. Idealized, discrete-circuit electrical analog for plate-like MnSi precipitates in Mn_nSi_{2n-m}.

flowing perpendicular to the c-axis. The MnSi will short out the resistance perpendicular to c, and

$$1/\rho_{\perp c} = (f/\rho_{\mathrm{MnSi}}) + [(1-f)/\rho_{Mn_nSi_{2n-m}}], \quad (1)$$

where f is the volume fraction of MnSi, and $\rho_{\perp c}$ is the *measured* resistivity of Mn_nSi_{2n-m} perpendicular to the c-axis. The corresponding shorting of $\rho_{\parallel c}$ is negligible.

Equation (1) implies that the true resistivity of Mn_nSi_{2n-m} perpendicular to c is about 20% higher than the measured $\rho_{\perp c}$, for $f = 0.02$. The measured $\rho_{\parallel c}$ is however a factor of 3 higher than $\rho_{\perp c}$. It would appear perhaps plausible to attribute the high measured $\rho_{\parallel c}$ to carrier scattering at faults at the MnSi–Mn_nSi_{2n-m} interface, but we cannot rule out an intrinsic resistivity anisotropy in Mn_nSi_{2n-m} proper. A similar analysis leads to similar conclusion regarding the thermal conductivity.

Using the schematic circuit of Fig. 6(b), it follows simply that $\alpha_{\perp c}$, the thermoelectric power of Mn_nSi_{2n-m} measured perpendicular to c, is given by

$$\alpha_{\perp c} = \alpha_{Mn_nSi_{2n-m}} + \frac{\rho_{Mn_nSi_{2n-m}}(\alpha_{\mathrm{MnSi}} - \alpha_{Mn_nSi_{2n-m}})}{\rho_{Mn_nSi_{2n-m}} + \rho_{\mathrm{MnSi}}(1-f)/f}. \quad (2)$$

From (2) we find (for $f = 0.02$) that the intrinsic thermoelectric power of Mn_nSi_{2n-m} perpendicular to c should be around 10% greater than the measured $\alpha_{\perp c}$, and thus, as for the resistivity, the effect of the MnSi precipitates is such as to tend to account for the observed anisotropy, but the calculated anisotropy is smaller than that observed. It is possible that the discrepancy arises from approximations made[4] in deriving (2), but once again an intrinsic anisotropy in α, though unusual, cannot be ruled out. If the thermoelectric power of Mn_nSi_{2n-m} were fairly isotropic, however, we would expect the intrinsic α for Mn_nSi_{2n-m} to be $\gtrsim \alpha_{\parallel c}$.

Using Table I, the measured thermoelectric figure of merit Z of Mn_nSi_{2n-m} at room temperature is[5]

$$Z = \alpha^2/\rho K \approx 2 \times 10^{-4}\ ^\circ\mathrm{K}^{-1},$$

both parallel and perpendicular to c. While clearly the effect of plate-like metallic MnSi precipitates ($Z_{\mathrm{MnSi}} \approx 5 \times 10^{-5}$) is to degrade the figure of merit of Mn_nSi_{2n-m}, from the above analysis we cannot evaluate the exact improvement in Z to be expected for Mn_nSi_{2n-m} grown by a method which avoids producing MnSi precipitates. However, if reasonably isotropic values of ρ, α, and K are typical of pure Mn_nSi_{2n-m}, we may estimate from the above[6]

$$Z_{Mn_nSi_{2n-m}} \approx \frac{(170 \times 10^{-6})^2}{1.1 \times 10^{-3} \times .05} \approx 6 \times 10^{-4}\ ^\circ\mathrm{K}^{-1},$$

i.e., an improvement of about a factor of 3 is possible.

7. Discussion

One major point which requires elaboration is the origin of the MnSi precipitates. From the phase diagram (Fig. 1), there is no reason to expect the appearance of MnSi *in* Mn_nSi_{2n-m} crystals. However, we have been unable to eliminate the precipitates from any of our melt-grown material. It is moreover clear from the published data that MnSi was present in Mn_nSi_{2n-m} produced by a number of workers (*7*, *10–12*, *18*) under varying conditions, and is probably inherent to all material produced by melt growth.

A hint as to the growth mechanism of MnSi precipitates can be found in their absence from the Mn_nSi_{2n-m}–Si eutectic phase (see Section 5).

[4] For example, the derivation of (2) assumes that electrical connection between the MnSi plates and the Mn_nSi_{2n-m} matrix is made only at the ends. Currents flowing between the two phases over the whole contact interface should degrade $\alpha_{\perp c}$ even more than that calculated.

[5] According to Ref. (*7*), Z increases by a factor of 2 on increasing the temperature to 400°C.

[6] We have used for this estimate $\alpha_{\parallel c}$, and values of $\rho_{\perp c}$ and $K_{\perp c}$ after correction for the shorting effect of the MnSi.

This would indicate that the presence of the nearby Si phase in the eutectic is such as to allow any MnSi to convert to Mn_nSi_{2n-m}, presumably by diffusion of Mn to the Si in the eutectic.

Another factor to bear in mind is the solubility range of Mn_nSi_{2n-m} necessarily implied by the varying superlattice structures. From the X-ray (*13–15*) and electron diffraction (*16*) results, we may denote the composition as $MnSi_{1.73+x}$, where x is a quasicontinuous variable with roughly $-0.02 < x < 0.02$. Melt-grown material will typically contain (*16*) a variety of the possible superstructures, and it is reasonable to expect the distribution of the various superstructures to be influenced by cooling rate and temperature, among other factors. The proper stoichiometry for a particular superstructure distribution could then be preserved by atomic diffusion, with excess Mn accumulating as the observed MnSi precipitates. It is interesting that the observed plate-like morphology of the precipitates, with the plane of the plates parallel to the (001) superlattice stacking plane, would fit such a picture. We may also add that the retrograde equilibrium solubility[7] of the type necessary to lead to MnSi precipitation has been observed (*6*) in the phase diagram of the defect semiconductor silicide $CrSi_2$.

To test the above ideas specimens of Mn_nSi_{2n-m} were sealed in evacuated quartz ampoules and subjected to annealing procedures. Annealing for 300 hr at 800°C and quenching into water produced no change in the microstructure [cf. Refs. (*7*, *18*)]. However, the result of annealing

[7] In $CrSi_2$, the equilibrium solubility range at low temperatures is silicon-rich compared to the as-grown stoichiometry at the melting point. This leads to CrSi precipitation.

FIG. 7. Melt-grown Mn_nSi_{2n-m} annealed 50 hr at 1130°C, and quenched. The MnSi precipitate spacing is around 20 μm. Figure 3 depicts the as-grown material before the quench–anneal procedure. As polished, polarized light, ×100.

for 50 hr at 1130°C (i.e., just below the peritectic decomposition) and quenching is given in Fig. 7. Figure 7 should be compared with Fig. 3, which illustrates the microstructure before the anneal–quench procedure. It is immediately apparent that the MnSi precipitates are present on a much finer scale. Low temperature magnetic measurements demonstrated that the volume fraction of MnSi was conserved.

We may estimate the order of magnitude of the diffusion coefficient D by

$$D \sim L^2/t, \tag{3}$$

where L is the characteristic length between the MnSi precipitates in Fig. 7 and t is the quench time, of the order of a few seconds. We find $D \sim 10^{-6}$ cm^2/sec. This value for D might appear overly high, but two comments are in order. First, the diffusion temperature was close to the peritectic temperature. Second, the diffusion of transition metals in Si and Ge is extremely high (*28*), with $10^{-6} < D < 10^{-4}$ typical at high temperatures. While, of course, Mn_nSi_{2n-m} is not tetrahedrally bonded as is Si, the Mn_nSi_{2n-m} lattice is not close packed. Each Si in the related $TiSi_2$ structure has only ten nearest neighbors, and the defect manganese silicide Mn_nSi_{2n-m} is even more open.

To confirm our analysis the quenched sample shown in Fig. 7 was reheated at 1130°C for 50 hr and then slowly oven-cooled. The MnSi precipitate spacing returned to the 100 μm value typical of Fig. 3, and incipient spheroidization was evident.

8. Summary

Low temperature magnetization measurements undertaken upon melt-grown single crystal Mn_nSi_{2n-m} have indicated that this material contains small quantities of MnSi precipitates independent of melt composition and growth parameters. From the data available in the literature (*7*, *10–12*, *18*) it appears that MnSi is invariably present in melt-grown Mn_nSi_{2n-m}.

Reported (*10–12*) magnetic data regarding Mn_nSi_{2n-m} is in fact characteristic of the MnSi precipitates. Mn_nSi_{2n-m} is diamagnetic at both room and liquid helium temperature.

Metallographic and electron microprobe studies have verified the presence of plate-like MnSi precipitates in an otherwise single crystal matrix of Mn_nSi_{2n-m}.

The precipitation of MnSi is diffusion controlled, and possibly related to the quasi-continuous stoichiometry range associated with the existence of a series of superstructures in Mn_nSi_{2n-m}.

Since MnSi is metallic, its presence degrades the thermoelectric figure of merit of Mn_nSi_{2n-m}. Some estimates are given of the probable effect of MnSi precipitates upon the electrical resistivity, thermal conductivity and thermoelectric power of the degenerate semiconductor Mn_nSi_{2n-m}.

Acknowledgments

Thanks are due to J. D. Livingston, G. A. Slack, and H. H. Woodbury for helpful discussions, and to R. G. Yelle for technical assistance.

References

1. R. K. Waits, *Proc. IEEE* **59**, 1425 (1971).
2. J. M. Andrews and F. B. Koch, *Solid State Electron.* **14**, 901 (1971).
3. G. V. Lashkarev and G. V. Samsonov, *Sov. At. Energy* **13**, 790 (1962).
4. R. M. Ware and D. J. McNeill, *Proc. Inst. Elec. Eng.* **111**, 178 (1964).
5. T. Tokushima, I. Nishida, K. Sakata, and T. Sakata, *J. Mater. Sci.* **4**, 978 (1969).
6. B. K. Voronov, L. D. Dudkin, N. I. Kiryukhina, and N. N. Trusova, *Izv. Akad. Nauk SSSR Neorg. Mater.* **4**, 325 (1968). [*Engl. Trans. Inorganic Materials* **4**, 271 (1968).]
7. L. D. Ivanova, N. Kh. Abrikosov, E. I. Elagina, and V. D. Khvostikov, *Izv. Akad. Nauk SSSR Neorg. Mater.* **5**, 1933 (1969). [*Engl. Trans. Inorganic Materials* **4**, 1645 (1969).]
8. E. N. Nikitin, V. I. Tarasov, and P. V. Tamarin, *Sov. Phys. Solid State* **11**, 187 (1969).
9. E. N. Nikitin, V. I. Tarasov, A. A. Andreev, and L. N. Shumilova, *Sov. Phys. Solid State* **11**, 2757 (1970).
10. I. Z. Radovskiy, F. A. Sidorenko, and P. V. Geld, *Fiz. Metal. Metalloved.* **19**, 514 (1965). [*Engl. Trans. Physics of Metals and Metallography* **19** (4), 30 (1965).
11. V. A. Korshunov, *Izv. Vyssh. Ucheb. Zaved. Fiz.* **11**, 131 (1968).
12. D. Shinoda and S. Asanabe, *J. Phys. Soc. Jap.* **21**, 555 (1966).
13. O. G. Karpinskii and B. A. Evseev, *Izv. Akad. Nauk SSSR Neorg. Mater.* **5**, 525 (1969). [*Engl. Trans. Inorganic Materials* **5**, 438 (1969).]
14. H. W. Knott, M. H. Mueller, and L. Heaton, *Acta Crystallogr.* **23**, 549 (1967).
15. G. Flieher, H. Vollenkle, and H. Nowotny, *Monatsh. Chem.* **98**, 2173 (1967).
16. R. De Ridder and S. Amelinckx, *Mater. Res. Bull.* **6**, 1223 (1971).

17. Y. FUJINO, D. SHINODA, S. ASANABE, AND Y. SASAKI, *Jap. J. Appl. Phys.* **3**, 431 (1964).
18. M. A. MOROKHOVETS, E. I. ELAGINA, AND N. KH. ABRIKOSOV, *Izv. Akad. Nauk SSSR Neorg. Mater.* **2**, 650 (1966). [*Engl. Trans. Inorganic Materials* **2**, 561 (1966).]
19. T. MAGER AND E. WACHTEL, *Z. Metallk.* **61**, 853 (1970).
20. H. F. STERLING AND R. W. WARREN, *Metallurgia* **67**, 301 (1963); D. W. OLIVER, G. D. BROWER, AND F. H. HORN, *J. Cryst. Growth* (in press).
21. G. ZWILLING AND H. NOWOTNY, *Monatsh. Chem.* **102**, 672 (1971).
22. U. BIRKHOLZ AND A. FRUEHAUF, *Phys. Status Solidi* **34**, K181 (1969).
23. I. Z. RADOVSKIY, F. A. SIDORENKO, AND P. V. GEL'D, *Fiz. Metal. Metalloved.* **19**, 915 (1965). [*Engl. Trans. Physics of Metals and Metallography* **19** (6), 104 (1965).]
24. H. J. WILLIAMS, J. H. WERNICK, R. C. SHERWOOD, AND G. K. WERTHEIM, *J. Appl. Phys.* **37**, 1256 (1966).
25. L. M. LEVINSON (unpublished).
26. F. I. OSTROVSKII, E. A. DMITRIEV, R. P. KRENTIS, AND P. V. GEL'D, *Izv. Vyssh. Ucheb. Zaved Fiz.* **12**, 108 (1969).
27. B. K. VORONOV, L. D. DUDKIN, AND N. N. TRUSOVA, *Sov. Phys. Crystallogr.* **12**, 448 (1967).
28. S. M. SZE, "Physics of Semiconductor Devices," p. 31. Wiley–Interscience, New York (1969).